



OPEN Differentiation of acute-phase AQP4-IgG+ optic neuritis from CNS inflammatory diseases using optic nerve head blood flow analysis

Chiaki Yamaguchi¹, Naoki Kiyota¹, Noriko Himori^{1,2}, Tatsuro Misu³, Kimihiko Kaneko³, Mizuki Otomo³, Airi Takagi¹, Takahiro Oshima¹, Ryo Kimura¹, Kazuko Omodaka¹, Satoru Tsuda¹, Masashi Aoki³ & Toru Nakazawa^{1,4,5,6}✉

Early diagnosis of optic neuritis (ON) associated with aquaporin-4 immunoglobulin-G (AQP4-IgG), myelin oligodendrocyte glycoprotein immunoglobulin-G (MOG-IgG), or multiple sclerosis (MS) is challenging due to invasive and time-consuming tests. We investigated whether ophthalmologic assessments, including laser speckle flowgraphy (LSFG) and optical coherence tomography (OCT), are useful for distinguishing among these diseases at ON onset. This retrospective study included 10 AQP4-IgG+ON patients, 20 MOG-IgG+ON patients, 9 MS-ON patients, and 27 idiopathic ON (ION) patients at initial onset, and 66 propensity-score-matched control eyes. We measured mean blur rate (MBR), representing blood flow velocity, using LSFG and assessed optic nerve head (ONH) vessel-area MBR (ONH-MV), tissue-area MBR (ONH-MT), and peripapillary choroidal MBR. Circumpapillary retinal nerve fiber layer (cpRNFL) thickness was measured with OCT. We found that MOG-IgG+ON patients had a significantly thicker cpRNFL than AQP4-IgG+ON patients and controls ($P < 0.05$). AQP4-IgG+ON and MOG-IgG+ON patients had significantly lower ONH-MV than controls ($P \leq 0.001$). AQP4-IgG+ON patients had significantly lower ONH-MT than MOG-IgG+ON, MS-ON, ION patients, or controls, and lower choroidal MBR than controls ($P < 0.05$). A receiver operating characteristic analysis combining cpRNFL thickness, ONH-MV, ONH-MT, and choroidal MBR achieved an area under the curve of 0.892 in differentiating AQP4-IgG+ON from other diseases ($P < 0.001$). LSFG and OCT could distinguish AQP4-IgG+ON from other diseases at onset non-invasively.

Keywords Laser speckle flowgraphy, Optic neuritis, Neuromyelitis optica spectrum disorders, Myelin oligodendrocyte antibody-associated diseases, Multiple sclerosis

Aquaporin-4 immunoglobulin G-positive (AQP4-IgG+) neuromyelitis optica spectrum disorder (NMOSD), myelin oligodendrocyte glycoprotein antibody-associated disease (MOGAD), and multiple sclerosis (MS) are autoimmune inflammatory diseases of the central nervous system (CNS), each characterized by a distinct pathophysiology, clinical features, and prognoses^{1–4}. AQP4-IgG+NMOSD is especially notable, as it targets astrocytes via complement-dependent and independent cell cytotoxicity and triggers secondary severe inflammation and demyelination, resulting in significant neurological impairments such as blindness, paralysis, and bladder dysfunction^{5–8}. Early diagnosis and timely treatment are essential; however, reliance on invasive and time-consuming tests, such as contrast-enhanced MRI and antibody assays, can delay intervention^{9,10}.

In these CNS diseases, inflammation often affects the optic nerves, leading to visual symptoms. Collaboration with ophthalmologists is thus crucial, as non-invasive and rapid ophthalmologic tests can help in the early differentiation of these CNS diseases, thereby improving the efficiency of clinical management. Previous studies have reported that the degree of optic nerve head (ONH) swelling, as measured by optical coherence tomography

¹Department of Ophthalmology, Tohoku University Graduate School of Medicine, 1-1 Seiryomachi, Aoba-Ku, Sendai, Miyagi 980-8574, Japan. ²Department of Aging Vision Healthcare, Tohoku University Graduate School of Biomedical Engineering, Sendai, Miyagi, Japan. ³Department of Neurology, Tohoku University Graduate School of Medicine, Sendai, Miyagi, Japan. ⁴Department of Ophthalmic Imaging and Information Analytics, Tohoku University Graduate School of Medicine, Sendai, Miyagi, Japan. ⁵Department of Retinal Disease Control, Tohoku University Graduate School of Medicine, Sendai, Miyagi, Japan. ⁶Department of Advanced Ophthalmic Medicine, Tohoku University Graduate School of Medicine, Sendai, Miyagi, Japan. ✉email: toru.nakazawa.e1@tohoku.ac.jp

(OCT), varies depending on the underlying CNS disease causing optic neuritis (ON)^{11–13}. Moreover, systemic vasculitis, such as in lupus or Sjögren syndrome, has been reported as a complication potentially related to the pathophysiology of AQP4-IgG+NMOSD, and the eye is the only organ where the vasculature can be observed and imaged in vivo through transparent tissues without invasive methods¹⁴. Laser speckle flowgraphy (LSFG) measures mean blur rate (MBR), a parameter corresponding to blood flow (BF) velocity, by utilizing speckle patterns generated by laser light scattered by moving red blood cells^{15–17}. LSFG is a non-invasive, efficient, and highly reproducible imaging modality that requires no dye and captures images within just four seconds^{15–17}. In a previous study using LSFG, we demonstrated reduced ocular BF in eyes with ON¹⁸. However, the underlying CNS disease-specific trends remain unclear.

In this study, we evaluated differences in circumpapillary retinal nerve fiber layer (cpRNFL) thickness and ocular BF among patients with AQP4-IgG+ON, MOG-IgG+ON, MS-ON, and idiopathic ON (ION) using OCT and LSFG. Through this evaluation, we aimed to investigate the potential utility of these measurements in differentiating underlying autoimmune inflammatory CNS diseases, particularly in supporting the diagnosis of AQP4-IgG+ON.

Results

A comparison of clinical characteristics and ophthalmological findings among the AQP4-IgG+ON, MOG-IgG+ON, MS-ON, ION, and control groups is presented in Table 1. There were no significant differences in the patient backgrounds of these groups ($P > 0.05$). The percentage of patients with ONH swelling was highest in the MOG-IgG+ON group and lowest in the AQP4-IgG+ON group, with a significant difference between these two groups (85.0% vs. 20.0%, $P < 0.001$). Compared to the control group, best-corrected visual acuity (BCVA) was worse in the AQP4-IgG+ON, MOG-IgG+ON, MS-ON, and ION groups ($P < 0.001$). The cpRNFL was thicker in the MOG-IgG+ON and ION groups than in the control group ($P < 0.001$), and it was thicker in the MOG-

Variables	ON groups, n = 66				Control, n = 66	P values	P values for specific pairs
	AQP4-IgG+ON	MOG-IgG+ON	MS-ON	ION			
Patients, (n, %)	10, (15.2%)	20, (30.3%)	9, (13.6%)	27, (40.9%)	–	–	–
Age, years	48.1 ± 19.0	49.1 ± 21.3	37.6 ± 12.0	40.1 ± 14.7	46.1 ± 16.8	0.222 [†]	
Male to female ratio	1:9	6:14	1:8	4:23	18:48	0.500	
Systolic BP, mmHg	126.50 ± 15.57	125.65 ± 22.58	122.78 ± 12.09	117.63 ± 16.58	121.14 ± 16.48	0.424 [†]	
Diastolic BP, mmHg	78.20 ± 11.45	73.05 ± 13.22	74.78 ± 6.67	72.63 ± 14.89	72.27 ± 11.21	0.683 [†]	
Pulse rate, bpm	76.50 ± 11.28	79.30 ± 13.85	78.00 ± 6.78	79.26 ± 15.46	75.91 ± 13.09	0.664 [‡]	
Hypertension (n, %)	3, (30.0%)	3, (15.0%)	1, (11.1%)	2, (7.4%)	13, (19.6%)	0.446	
Diabetes mellitus (n, %)	0, (0.0%)	0, (0.0%)	0, (0.0%)	0, (0.0%)	5, (7.6%)	0.498	
Dyslipidemia (n, %)	3, (30.0%)	3, (15.0%)	0, (0.0%)	1, (3.7%)	13, (19.6%)	0.111	
Heart disease (n, %)	0, (0.0%)	0, (0.0%)	0, (0.0%)	0, (0.0%)	6, (9.1%)	0.345	
Optic disc swelling (n, %)	2, (20.0%)	17, (85.0%)	6, (66.7%)	15, (55.5%)	–	0.005	E < 0.001 ^{*,*}
Length of the ON lesion, mm	28.35 ± 12.97	23.77 ± 11.06	20.02 ± 6.29	19.20 ± 8.26	–	0.325	
ON localization							
Intraorbital (n, %)	5/9, (55.6%)	19/20, (95.0%)	7/8, (87.5%)	23/27, (85.2%)	–	0.076	
Canalicular (n, %)	7/9, (77.8%)	6/20, (30.0%)	2/8, (25.0%)	9/27, (33.3%)	–	0.077	
Pre-chiasmatal (n, %)	5/9, (55.6%)	6/20, (30.0%)	2/8, (25.0%)	5/27, (18.5%)	–	0.233	
Chiasmatal (n, %)	3/9, (33.3%)	4/20, (20.0%)	1/8, (12.5%)	6/27, (22.2%)	–	0.801	
Optic tract (n, %)	1/9, (11.1%)	0/20, (0.0%)	0/8, (0.0%)	0/27, (0.0%)	–	0.266	
BCVA, logMAR	1.81 ± 1.20	1.16 ± 1.00	0.78 ± 0.75	1.22 ± 1.12	–0.12 ± 0.08	< 0.001 ^{‡,*}	A, B, C, D < 0.001 ^{*,*}
IOP, mmHg	15.87 ± 2.82	15.68 ± 3.46	16.46 ± 3.46	15.99 ± 2.37	15.38 ± 3.10	0.918 [†]	
Color vision, Ishihara score	3.33 ± 6.63	4.21 ± 6.39	6.00 ± 7.30	5.54 ± 6.95	–	0.547 [‡]	
CpRNFL thickness, μm	113.68 ± 22.55	167.99 ± 62.06	125.17 ± 30.94	155.65 ± 89.95	104.59 ± 11.73	< 0.001 ^{‡,*}	B, D < 0.001 ^{*,*} , E = 0.002 ^{*,*}
Time before OCT, days	3.20 ± 3.36	3.05 ± 3.49	6.78 ± 3.31	4.22 ± 3.98	–	0.075 [‡]	
Time before LSFG, days	3.40 ± 3.20	3.15 ± 3.59	7.11 ± 3.48	4.78 ± 4.02	–	0.054 [‡]	

Table 1. Comparison of clinical characteristics among AQP4-IgG+ON, MOG-IgG+ON, MS-ON, ION, and control groups. A, AQP4-IgG+ON versus control; B, MOG-IgG+ON versus control; C, MS-ON versus control; D, ION versus control; E, AQP4-IgG+ON versus MOG-IgG+ON. AQP4, aquaporin-4; BCVA, best-corrected visual acuity; BP, blood pressure; CpRNFL, circumpapillary retinal nerve fiber layer; IgG, immunoglobulin G; ION, idiopathic optic neuritis; IOP, intraocular pressure; LSFG, laser speckle flowgraphy; MOG, myelin oligodendrocyte glycoprotein; MS, multiple sclerosis; OCT, optical coherence tomography; ON, optic neuritis. P value indications: * indicates statistical significance after appropriate corrections. Unmarked P values: chi-square test; † indicates one-way analysis of variance (ANOVA) and ‡ indicates Kruskal–Wallis test. For pairwise comparisons, § indicates the Tukey test, ¶ the Dunn test, and # the Fisher exact test. The significance level for the Dunn, chi-square, and Fisher exact tests was set at $P < 0.005$ after Bonferroni correction.

IgG+ON group than the AQP4-IgG+ON group ($P=0.002$). There were no significant differences in intraocular pressure (IOP) ($P=0.918$).

Figure 1 shows box plots of LSF-G-derived parameters for the control and ON-related CNS disease groups. The MOG-IgG+ON group showed a significant decrease in ONH vessel-area mean blur rate (MBR; ONH-MV) compared to the control group ($P<0.001$). The AQP4-IgG+ON group also showed a significant decrease in ONH-MV compared to the control group ($P=0.001$), but there was no significant difference between the AQP4-IgG+ON and MOG-IgG+ON groups (Fig. 1a). The AQP4-IgG+ON group showed a significant decrease in ONH tissue area MBR (ONH-MT), which reflects circulation in the deep capillaries, compared to the MOG-IgG+ON, MS-ON, ION, and control groups ($P=0.010$, $P=0.039$, $P=0.015$, and $P=0.004$, respectively) (Fig. 1b). The AQP4-IgG+ON group showed a significant reduction in peripapillary choroidal MBR compared to the control group ($P<0.001$) after Bonferroni correction (Fig. 1c).

Representative control cases and cases of each ON-related CNS disease are shown in Fig. 2. Cases are shown from top to bottom, as follows: AQP4-IgG+ON, MOG-IgG+ON, MS-ON, ION, and control. In fundus photographs and OCT images, ONH swelling was observed in the MOG-IgG+ON, MS-ON, and ION patients but not in the AQP4-IgG+ON patient. In the LSF-G color maps, the AQP4-IgG+ON patient showed decreased MBR in the central retinal artery region, as well as decreased ONH tissue area and peripapillary choroidal MBR, which can be seen by the cooler colors in comparison to other ON-related CNS diseases and the control case.

Figure 3 shows the receiver operating characteristic (ROC) curves for distinguishing AQP4-IgG+ON from other ON-related CNS diseases using different modalities. The area under the curve (AUC) was 0.739 (95% CI 0.574–0.903; $P=0.086$) for OCT alone (cpRNFL thickness) and 0.873 (95% CI 0.772–0.974; $P<0.001$) for LSF-G parameters alone. When cpRNFL thickness and LSF-G parameters were combined, the AUC reached 0.892 (95% CI 0.764–0.999; $P<0.001$), which was the highest diagnostic performance among all models and exceeded the performance of either modality alone.

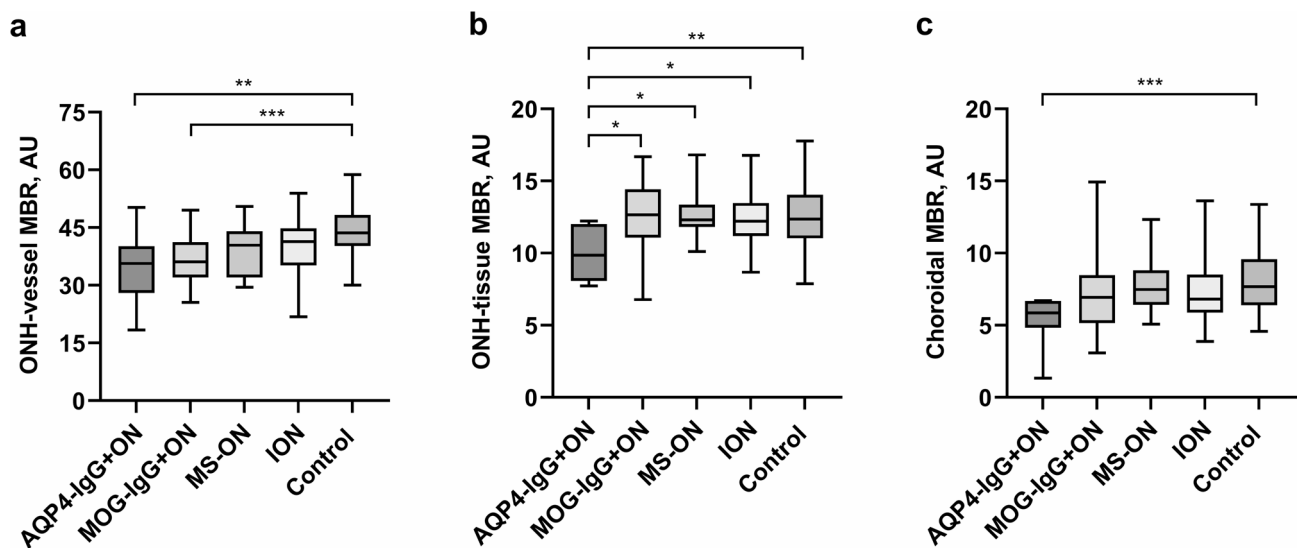


Fig. 1. Box plots for LSF-G parameters in the AQP4-IgG+ON, MOG-IgG+ON, MS-ON, control, and ION groups. The x-axis shows the diagnosis, and the y-axis shows the MBR values. Left to right: ONH-MV, ONH-MT, and peripapillary choroidal MBR. **(A)** ONH-MV. The ONH-MV values are as follows: AQP4-IgG+ON group, 34.58 ± 8.99 arbitrary units (AU); MOG-IgG+ON group, 36.74 ± 6.16 AU; MS-ON group, 38.93 ± 7.02 AU; ION group, 40.07 ± 7.77 AU; and control group, 43.87 ± 6.45 AU (overall $P<0.001$). Comparisons of groups are as follows: AQP4-IgG+ON with MOG-IgG+ON ($P=0.924$), MS-ON ($P=0.637$), ION ($P=0.200$), and control ($P=0.001$); MOG-IgG+ON with MS-ON ($P=0.931$), ION ($P=0.469$), and control ($P<0.001$); MS-ON with ION ($P=0.992$) and control ($P=0.257$); and ION with control ($P=0.117$). **(B)** ONH-MT. The ONH-MT values are as follows: AQP4-IgG+ON group, 9.97 ± 1.85 AU; MOG-IgG+ON group, 12.62 ± 2.54 AU; MS-ON group, 12.68 ± 1.84 AU; ION group, 12.42 ± 1.83 AU; and control group, 12.52 ± 2.07 AU (overall $P=0.009$). Comparisons of groups are as follows: AQP4-IgG+ON with MOG-IgG+ON ($P=0.010$), MS-ON ($P=0.039$), ION ($P=0.015$), and control ($P=0.004$); MOG-IgG+ON with MS-ON ($P=0.999$), ION ($P=0.997$), and control ($P>0.999$); MS-ON with control ($P>0.999$) and ION ($P=0.997$); and ION with control ($P>0.999$). **(C)** Peripapillary choroidal MBR. The peripapillary choroidal MBR values are as follows: AQP4-IgG+ON group, 5.37 ± 1.62 AU; MOG-IgG+ON group, 7.44 ± 3.05 AU; MS-ON group, 7.79 ± 2.10 AU; ION group, 7.25 ± 2.09 AU; and control group, 8.11 ± 2.11 AU (overall $P=0.004$). Comparisons of groups are as follows: AQP4-IgG+ON with MOG-IgG+ON ($P=0.171$), MS-ON ($P=0.074$), ION ($P=0.109$), and control ($P<0.001$); MOG-IgG+ON with MS-ON ($P>0.999$), ION ($P>0.999$), and control ($P=0.446$); MS-ON with ION ($P>0.999$) and control ($P>0.999$); and ION with control ($P=0.401$). All P values are after Bonferroni adjustment. * $P<0.05$, ** $P<0.01$, *** $P<0.001$.

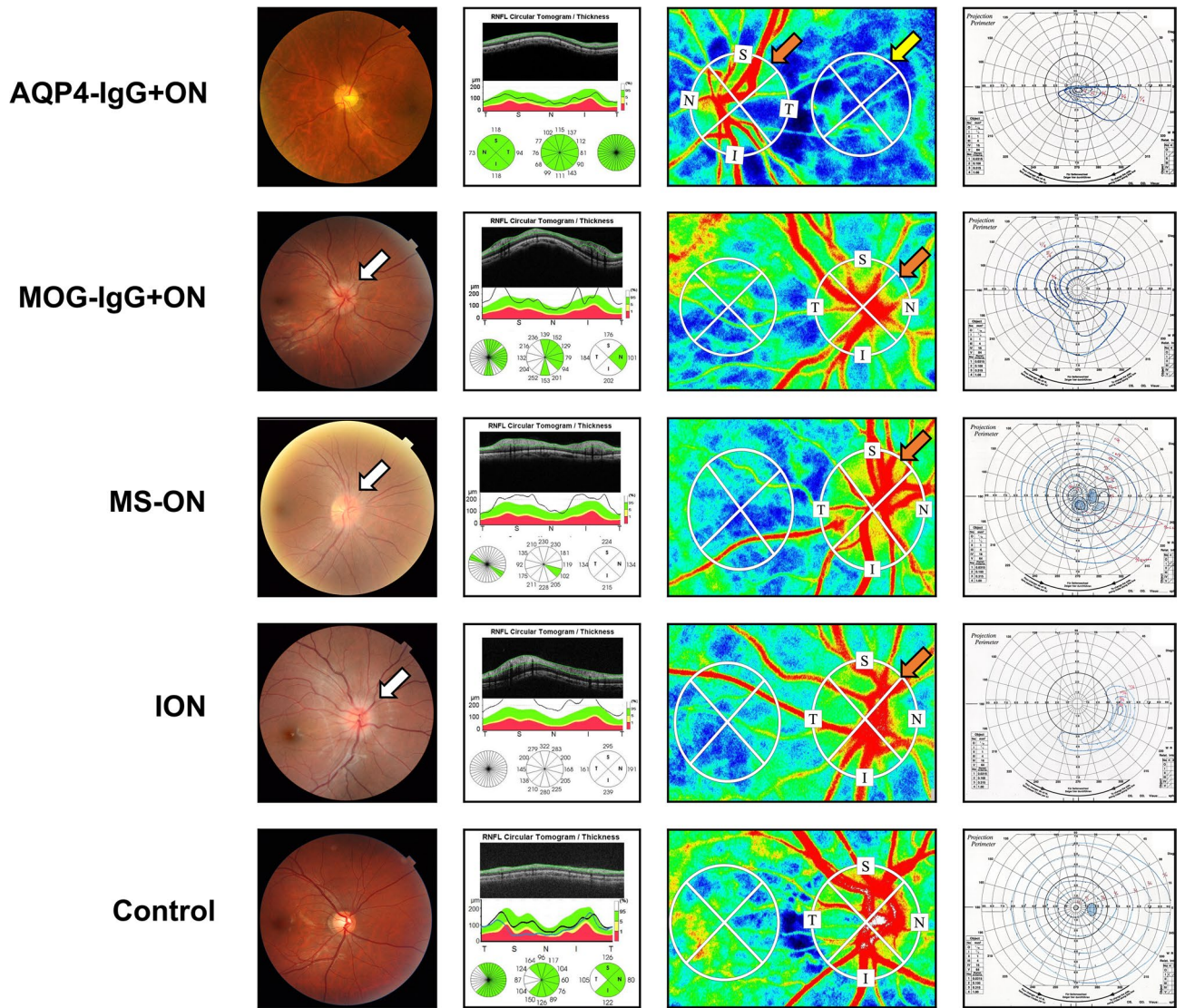


Fig. 2. Ocular examination data from representative cases. The examinations include, from left to right, the following: fundus photographs, OCT images, LSF color map images, and Goldmann kinetic perimetry (GP). AQP4-IgG+ON patient: BCVA is 20/40, and IOP is 16.7 mmHg. The fundus photograph and OCT image are normal. The ONH large vessel area, tissue area, and choroidal area (orange and yellow arrows) show decreased BF; ONH-MV is 30.8 AU, ONH-MT is 8.5 AU, and peripapillary choroidal MBR is 5.0 AU. A superior visual field defect is present in the GP. MOG-IgG+ON patient: BCVA is 20/400, IOP is 20.3 mmHg. ONH swelling is present in the fundus photograph (white arrow) and OCT image. In the LSF color map, the boundary between the large vessel and tissue areas within the ONH is obscured (orange arrow); ONH-MV is 30.6 AU, ONH-MT is 14.4 AU, peripapillary choroidal MBR is 6.3 AU. The GP data show a central scotoma. MS-ON patient: BCVA is 20/13, IOP is 13.0 mmHg. ONH swelling is observed in the fundus photograph (white arrow) and OCT image. In the LSF color map, the boundary between the large vessel and tissue areas within the ONH is blurred (orange arrow); ONH-MV is 34.3 AU, ONH-MT is 12.8 AU, choroidal MBR is 7.3 AU. The GP show a parafoveal scotoma. ION patient: BCVA is counting fingers at 10 cm, and IOP is 14.7 mmHg. ONH swelling is observed in the fundus photograph (white arrow) and OCT image. In the LSF color map, the boundary between the large vessel and tissue areas within the ONH is blurred (orange arrow); ONH-MV is 29.5 AU, ONH-MT is 12.4 AU, and peripapillary choroidal MBR is 7.2 AU. Almost complete visual field loss is shown by the GP. Control: The fellow eye of a patient with normal tension glaucoma. BCVA is 20/16, and IOP is 12.0 mmHg. The fundus photograph and OCT image are normal. The LSF color map is normal: ONH-MV is 55.4 AU, ONH-MT is 14.3 AU, and peripapillary choroidal MBR is 10.1 AU. The GP is normal.

Discussion

This study is an evaluation of differences in the degree of ONH swelling and BF reduction at initial onset among CNS diseases presenting with ON and to demonstrate the potential utility of these parameters for differential diagnosis. The MOG-IgG+ON group showed severe thickening of the cpRNFL compared to the AQP4-IgG+ON

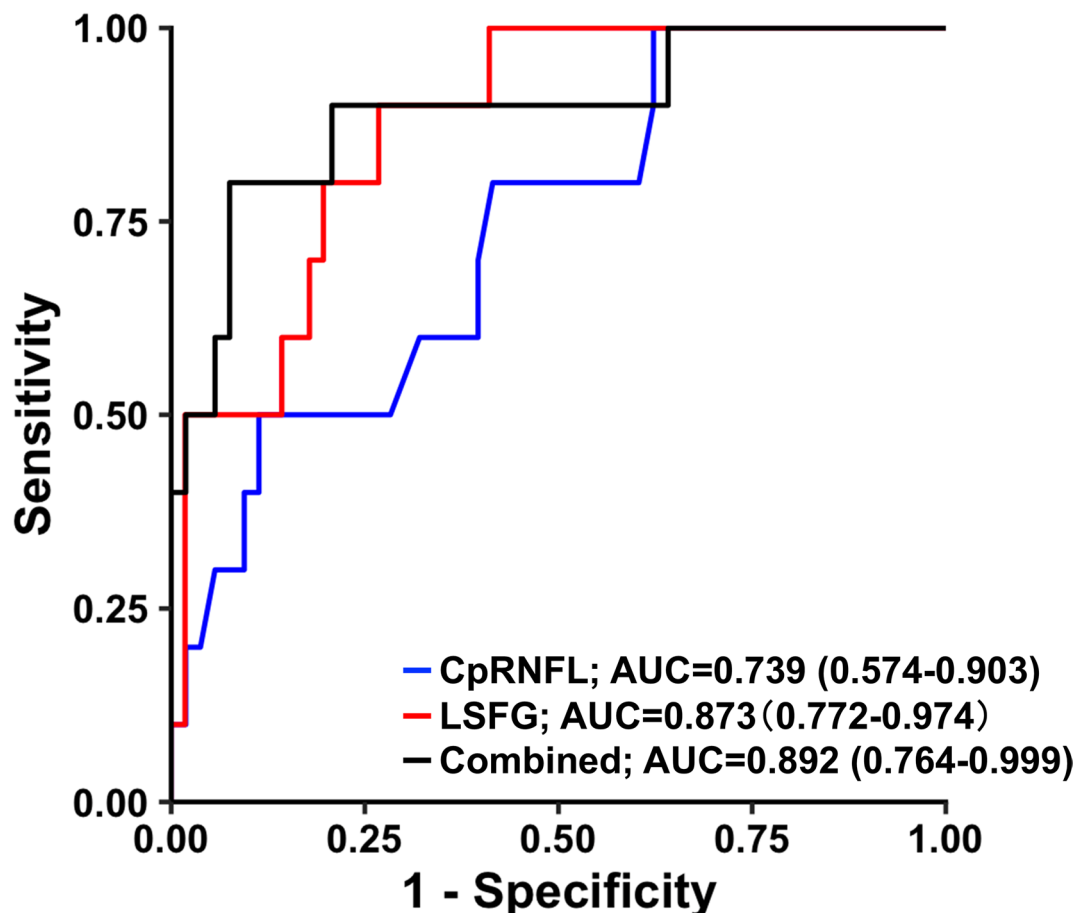


Fig. 3. ROC curves for differentiating AQP4-IgG+ON from other ON-related CNS diseases (MOG-IgG+ON, MS-ON, and ION), based on standardized cpRNFL thickness, ONH-MV, ONH-MT, and peripapillary choroidal MBR. The AUC was 0.739 (95% CI 0.574–0.903; $P=0.086$) for OCT alone (cpRNFL thickness; blue), and 0.873 (95% CI 0.772–0.974; $P<0.001$) for LSF parameters alone (red). When cpRNFL thickness and LSF parameters were combined (black), the AUC reached 0.892 (95% CI 0.764–0.999; $P<0.001$).

and control groups. In contrast, the AQP4-IgG+ON group showed a decrease in BF in the large vessel, capillary, and peripapillary choroidal areas of the ONH compared to the control group. In addition, the AQP4-IgG+ON group showed a decrease in ONH capillary BF compared to the MOG-IgG+ON, MS-ON, and ION groups, suggesting that a unique mechanism of hypoperfusion is related to tissue injury in AQP4-IgG+NMOSD. It was possible to differentiate AQP4-IgG+ON from other ON-related CNS diseases using OCT and LSF parameters, which could contribute to the diagnosis of AQP4-IgG+NMOSD in patients in whom it is difficult to identify this disease at its initial onset.

In this study, the AQP4-IgG+ON group showed a decrease in BF in the ONH large vessels, ONH capillaries, and peripapillary choroid. Also, the MOG-IgG+ON group showed more severe ONH swelling than the AQP4-IgG+ON group, as well as decreased BF in the ONH large vessels, but not in the ONH capillaries, compared to the control group, suggesting that there are different mechanisms of tissue edema and damage in AQP4-IgG+disease and MOG-IgG+disease. AQP4 is a water channel expressed in the foot processes of astrocytes and is considered a primary target in AQP4-IgG+NMOSD^{19–21}. In AQP4-IgG+NMOSD, AQP4-IgG and its activated complement are deposited around blood vessels and in the astrocytic foot processes, leading to primarily astrocyte lysis at the perivascular areas, disrupting the vascular barrier function and increasing the permeability of the blood–brain barrier, which leads to astrocytopathic tissue injury and vasogenic edema^{8,22,23}. This astrocytopathic lesion with loss of AQP4 and astrocytes causes a secondary demyelinating lesion, featuring dominant loss of myelin-associated glycoprotein, which is a typical ischemia-like pattern of demyelination related to astrocyte loss and microvasculature change in AQP4-IgG+NMOSD^{6,24}. Therefore, the specific underlying tissue injury in AQP4-IgG+NMOSD could explain the differences in BF and ONH changes compared with MOGAD in the present study. In addition, focal tissue injury induces the production of inflammatory cytokines such as IL-6 and the recruitment of chemokines, promoting the infiltration of inflammatory cells and the progression of inflammation; nevertheless, increased levels of cerebrospinal fluid cytokines such as IL-6 are commonly observed in the acute stage of AQP4-IgG+NMOSD and MOGAD^{8,22,23,25,26}.

Astrocytes are present in the retina in addition to the optic nerve, which suggests that the retina is the primary target of AQP4 antibodies, causing retinitis with axonal pathology in the RNFL and ganglion cell layer^{27,28}.

Furthermore, it is reasonable that BF derived from the central retinal artery and short posterior ciliary artery is affected, possibly because complication with systemic vasculitis which is occasionally observed in AQP4-IgG+NMOSD, or because the possible mechanisms of astrocyte dysfunction and vasodynamic change cause tissue edema and necrosis, as discussed in ischemic models of AQP4 depolarization²⁹.

In AQP4-IgG+ON, inflammation tends to occur posterior to the optic nerve, including in the optic chiasm and optic tract, more frequently than in other types of ON. In contrast, in MOG-IgG+ON, inflammation tends to occur from the optic nerve to near the ONH^{30,31}, which is one of the causes of MOG-IgG+ON mainly occurring with ONH swelling. It is known that in anterior ON, in which ONH swelling occurs, the boundary between the ONH vessels and tissue is blurred³², and under these circumstances, ONH-MV is markedly reduced, while ONH-MT is relatively unaffected, which is consistent with our findings³³.

The MS-ON patients in this study did not show significant BF impairment compared to the control group or the groups with other ON-related CNS diseases. In MS, demyelinating lesions in the CNS are the predominant pathology, and blood–brain barrier damage, increased vascular permeability, and perivascular inflammation are not as severe as seen in MOGAD and AQP4-IgG+NMOSD^{34,35}. Therefore, it is possible that this explains why BF damage was not observed in either the ONH or peripapillary choroidal regions in our LSFSG evaluations.

In this study, a model using cpRNFL thickness and LSFSG parameters (ONH-MV, ONH-MT, and peripapillary choroidal MBR) showed high diagnostic accuracy (AUC=0.892) in discriminating AQP4-IgG+ON from other ON-related CNS diseases. Other diagnostic methods, such as those based on contrast-enhanced MRI (AUC=0.876) and the urine proteome (AUC=0.858), are useful, but they have limitations such as invasiveness and being time consuming^{36,37}. Alternative methods using simpler ophthalmic devices, such as OCT angiography (OCTA), have been reported. For the differentiation of AQP4-IgG+ON and MS-ON, analyses of vessel density and perfusion density (AUC=0.857)³⁸, the combination of OCTA and serum markers (AUC=0.813)³⁹, and sector-based methods focusing on patterns of vessel density reduction (AUC=0.833)⁴⁰ have been highlighted as effective. However, studies using OCTA have primarily focused on chronic-phase BF and used methods that were not specialized for acute-phase diagnosis. Furthermore, there have been no reports that included MOG-IgG+ON. To address these gaps, our study aimed to improve the early diagnosis of CNS diseases causing ON by focusing on and collecting cases in the initial and early stages. A key strength of our study lies in including patients with MOG-IgG+ON, which requires antibody testing, thereby broadening the scope of diagnostic evaluation.

In the 2024 revision of the McDonald diagnostic criteria¹³, the optic nerve was added as the fifth anatomical region of the CNS. Results from evaluation of the optic nerve using OCT, visual evoked potential, and orbital MRI are now recognized as valid evidence for determining dissemination in space. In this study, we focused on the acute phase of ON, and the OCT findings we assessed—namely, transient thickening due to edema—differ from those considered in the McDonald criteria, which include chronic damage, manifested as thinning. Nevertheless, this revision aligns with our findings in highlighting the growing importance of ocular assessment in CNS inflammatory diseases.

This study has several limitations. First, this was a relatively short-term study, and the proportions of patients with different causes of ON may have differed in a longer-term study. However, ON is a rare disease, and large-scale surveys focusing on ON with specific conditions, such as BF measurements and antibody testing, are limited in Japan. Therefore, we consider that this study provides important evidence on MOG-IgG and AQP4-IgG antibodies and ocular BF measurements. Second, the diagnosis of ION in this study was based only on brain MRI and serological testing. We did not perform cerebrospinal fluid analysis including testing for oligoclonal bands due to its invasiveness; moreover, spinal MRI has low utility for rare asymptomatic cases of myelitis. Therefore, we cannot completely rule out the possibility that the ION group included patients who currently had seronegative NMOSD or who may be diagnosed with MS in the future. Third, it is not fully understood whether LSFSG reflects BF in deeper or more superficial areas. ONH-MT has been reported to reflect deep-tissue-area BF^{41,42}, but it may also include more superficial BF, and ONH-MV may reflect some degree of BF in deeper areas. A newly developed LSFSG device with depth information would be ideal. Fourth, since this was a cross-sectional study, it is unclear whether the LSFSG parameters can be used as disease state markers or for making prognoses. Especially, it is limited in considering the tissue pathology using this kind of in-direct methodology. However, the significant decrease of BF in NMOSD is observed without RNFL thickness change, so we consider it could not simply be discussed as a secondary phenomenon of tissue damage. Fifth, the possibility that optic disc edema affected the LSFSG measurements cannot be excluded. Nevertheless, the presence of clear intergroup differences based on the measured values indicates that LSFSG is useful for differentiating AQP4-IgG+ON from other diseases. Whether BF in AQP4-IgG+ON is in fact reduced to the extent measured in this study will require further advances in technology to determine. Sixth, OCTA data were not available for this study, which limited our ability to comprehensively evaluate vascular structure. While OCTA is suitable for detecting vascular structural changes, LSFSG allows for assessment of BF; each modality has its own advantages. In the future, a combined approach using both LSFSG and OCTA may provide a more comprehensive understanding of the pathophysiology of ON.

In conclusion, this study demonstrated that ocular non-invasive examination parameters, such as OCT and LSFSG, can potentially aid in differentiating ON-related CNS diseases; in particular, they can distinguish AQP4-IgG+ON from other ON-related CNS diseases.

Materials and methods

This was a retrospective, cross-sectional study conducted at Tohoku University Hospital in Sendai, Miyagi, Japan. The institutional review board of the Tohoku University Graduate School of Medicine approved the study. All procedures were approved by the ethics committee of Tohoku University Graduate School of Medicine and conformed with the Declaration of Helsinki and its later amendments or comparable ethical standards. The

Study Flow at Tohoku University Hospital (June 2012–April 2024)

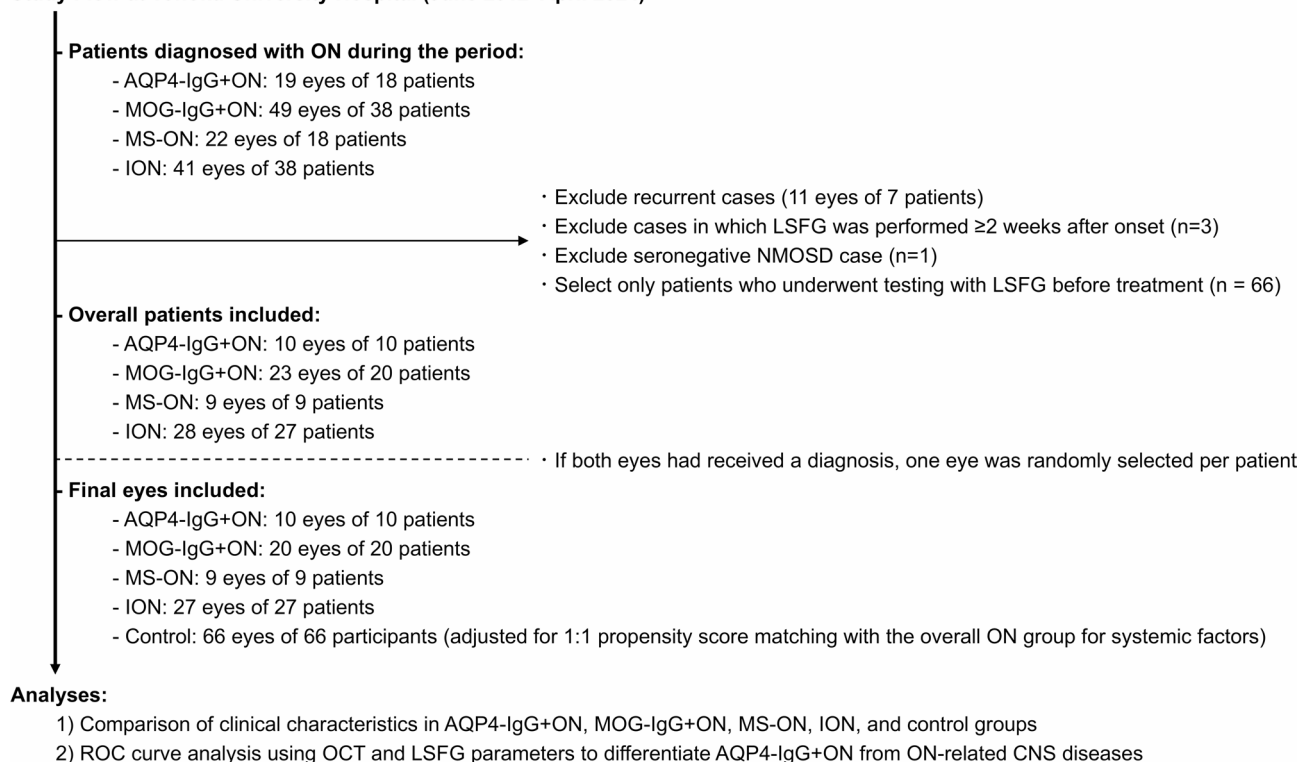


Fig. 4. Criteria for eye selection in this study. The horizontal arrows indicate the exclusion criteria. AQP4-IgG+, aquaporin-4 immunoglobulin G-positive; ION, idiopathic optic neuritis; LSF, laser speckle flowgraphy; MOG-IgG+, myelin oligodendrocyte glycoprotein immunoglobulin G-positive; MS, multiple sclerosis; NMOSD, neuromyelitis optica spectrum disorder; OCT, optical coherence tomography; ON, optic neuritis.

criteria for eye selection in this study are shown in Fig. 4. We reviewed medical records from June 2012 to April 2024 and identified 18 patients with AQP4-IgG+ON, 38 patients with MOG-IgG+ON, 18 patients with MS-ON, and 38 patients with ION. Only patients with initial-onset ON who had not yet started treatment were included in this study. We excluded cases of recurrent ON, cases of seronegative NMOSD, cases in which the patient did not undergo LSF imaging before treatment, and cases in which LSF imaging was performed 2 or more weeks after ON onset. If both eyes were diagnosed, one eye was randomly selected per subject. Finally, the analysis included 10 affected eyes of 10 AQP4-IgG+ON patients, 20 affected eyes of 20 MOG-IgG+ON patients, 9 affected eyes of 9 MS-ON patients, and 27 affected eyes of 27 ION patients. ON and its underlying CNS diseases were diagnosed by a neuro-ophthalmologist (N.H.) and a neurologist (T.M.). The inclusion criteria for ON were as follows: (1) acute visual disturbance or visual field defect; (2) relative afferent pupillary defect; (3) reduced critical flicker fusion frequency; (4) contrast effects along the optic nerve in contrast-enhanced MRI; and (5) no evidence of any other neurologic, infectious, or neoplastic ocular disease that could be responsible for visual impairment.

The microscopic live cell-based assay method was used to confirm MOG-Ab/AQP4-Ab positivity in the serum and cerebrospinal fluid^{43,44}. Human M23-AQP4 or human MOG-expressing HEK293 cells were incubated with diluted serum samples taken from the patients. A secondary antibody specific to the IgG-Fc fragment was used. Serum samples were screened at dilutions of 1:16 for AQP4-Ab and 1:128 for MOG-Ab. Cerebrospinal fluid samples were screened without diluting the samples in either of the antibodies. The treated cells were stained with an Alexa Fluor 488-conjugated anti-human IgG Fc fragment secondary antibody (Thermo Fisher Scientific, Waltham, MA, USA). The titrations were evaluated visually semi-quantitatively using consecutive twofold end-point dilutions. MOG-IgG+ON patients were diagnosed based on the criteria proposed by the 2023 International MOGAD Panel⁴⁵. AQP4-IgG+ON patients were diagnosed according to the 2015 International Panel for NMO Diagnosis criteria⁴⁶. MS-ON patients met the 2017 revised McDonald criteria⁴⁷. Patients with ON were classified as having ION if they tested negative for both anti-MOG and anti-AQP4 antibodies, they did not meet the criteria for MS, and secondary causes of ON were ruled out³.

We interviewed each patient at the initial onset of ON for a detailed medical history; details recorded included the presence of hypertension (HT), diabetes mellitus (DM), dyslipidemia (DL), and heart disease (HD). Baseline data were collected, including visual acuity, IOP, slit lamp findings, and a dilated funduscopic examination. The control group was selected by 1:1 propensity matching adjusted for age, gender, systolic blood pressure (BP), diastolic BP, pulse rate (PR), HT, DM, DL, and HD for the ON group. The control group included 66 fellow eyes of patients with cataracts, glaucoma, epiretinal membrane, or traumatic optic neuropathy. We did not observe

evident thinning of the cpRNFL ($104.59 \pm 11.73 \mu\text{m}$) or glaucomatous visual field defects (mean deviation: $-0.73 \pm 1.54 \text{ dB}$) in the fellow control eyes of the patients with glaucoma. The analyses in this study included (1) a comparison of systemic and ocular parameters among the AQP4-IgG+ON, MOG-IgG+ON, MS-ON, ION, and control groups, and (2) ROC curve analysis using OCT and LSFSG parameters to differentiate AQP4-IgG+ON from other ON-related CNS diseases.

Measurement of clinical variables and BF parameters

The length of the ON lesion in orbital MRI images was semi-quantitatively represented by the number of segments showing involvement in the following five areas of the optic nerve: intraorbital, canalicular, pre-chiasmal, chiasmal, and optic tract³⁶. The BCVA was used and converted to the logarithmic minimum angle of resolution (logMAR) for analysis. IOP was measured with non-contact tonometry (Tonoref III; Nidek Co., Ltd, Gamagori, Japan). Color vision was assessed using the Ishihara test. Visual field testing was performed with Goldmann kinetic perimetry. The cpRNFL thickness was determined with the 3D OCT-2000-embedded software (ver. 8.11, Topcon Corporation, Tokyo, Japan). ONH and choroidal BF were assessed with the LSFSG-NAVI device (Softcare Co., Ltd., Fukutsu, Japan), which measures MBR in arbitrary units. First, an ellipsoid was manually drawn around the ONH to define the region of interest (ROI) in composite MBR color maps. The accompanying LSFSG software (LSFSG analyzer, version 3.1.59.0) then automatically divided the large-vessel and tissue (i.e., capillary) areas of the ONH and determined MV and MT separately in a cross-sectional analysis. ONH-MT has been reported to be a good indicator of BF in the deep capillaries of the ONH^{41,42}. A same-sized ROI was then set on the temporal side of the ONH in the same image to mark the choroidal region, as we described previously^{18,48,49}. The ONH-MV reflects BF derived from the central retinal artery, while ONH-MT and peripapillary choroidal MBR reflect BF derived from the short posterior ciliary artery^{41,42}. Before the LSFSG measurements, the patient's pupils were dilated with 0.4% tropicamide, a muscarinic antagonist (Mydrin M; Santen Pharmaceutical Co., Ltd). After the instillation, the patient sat in a dark, quiet room for 15 min to stabilize pupil dilation, BP, and PR. Then, BP and PR were measured (HBP-1300; Omron Colin Co., Ltd. Tokyo, Japan), and LSFSG was performed.

Statistical analysis

The target sample size was calculated based on the between-group difference in peripapillary choroidal MBR reported in a previous study¹⁸. Specifically, we assumed that tests to compare the five groups had a standard deviation of 2–3, a statistical power of 80%, and a two-sided significance level of 5%. Calculations were performed using SAS version 9.4 (SAS Institute, Cary, NC, USA). Since the prevalence of ON varies depending on the underlying CNS disease^{2,50}, and AQP4-IgG+ON and MS-ON were relatively rare in this study, the AQP4-IgG+ON to MOG-IgG+ON to MS-ON to ION to control allocation ratio was set at 1:2:1:3:7 in consideration of the differences in the number of cases among these groups.

All data are shown as the mean value \pm SD. Shapiro–Wilk and Levene tests were performed to confirm the normality of continuous variables in all analyses. Based on these results, the Kruskal–Wallis test was used to analyze the overall group, with the Dunn post-hoc test used for pairwise comparisons. For analyses using a one-way analysis of variance (ANOVA), the Tukey honestly significant difference (HSD) test was performed as a post-hoc analysis. For comparisons of continuous variables between pairs of groups after propensity matching, the t-test was used for parametric variables, and the Wilcoxon rank sum test was used for nonparametric variables. For nominal variables, chi-square tests and Fisher exact tests were used. The significance level for overall group comparisons was set at $P < 0.05$. Using Bonferroni correction, the significance levels for the Dunn post-hoc test for pairwise comparisons and Fisher exact test were adjusted to $P < 0.005$.

ROC curve analysis was performed to evaluate the diagnostic ability of the examined parameters for AQP4-IgG+ON and other ON-related CNS diseases, including a combination of standardized cpRNFL thickness, ONH-MV, ONH-MT, and peripapillary choroidal MBR parameters. The AUC was calculated to quantify the model's discriminative power and assess the diagnostic ability for AQP4-IgG+ON compared to other ON-related CNS diseases. All statistical analyses were performed with R software version 4.4.2 (available at <https://www.R-project.org/>).

Data availability

The datasets either used or analyzed or both in the current study are available from the corresponding author upon reasonable request.

Received: 2 May 2025; Accepted: 5 September 2025

Published online: 29 September 2025

References

- Hassan, M. B. et al. Population-based incidence of optic neuritis in the era of aquaporin-4 and myelin oligodendrocyte glycoprotein antibodies. *Am. J. Ophthalmol.* **220**, 110–114 (2020).
- Ishikawa, H. et al. Epidemiologic and clinical characteristics of optic neuritis in Japan. *Ophthalmology* **126**(10), 1385–1398 (2019).
- Toosy, A. T., Mason, D. F. & Miller, D. H. Optic neuritis. *Lancet Neurol.* **13**(1), 83–99 (2014).
- Bennett, J. L. et al. Optic neuritis and autoimmune optic neuropathies: Advances in diagnosis and treatment. *Lancet Neurol.* **22**(1), 89–100 (2023).
- Vanikieti, K. et al. Clinical characteristics and long-term visual outcome of optic neuritis in neuromyelitis optica spectrum disorder: A comparison between Thai and American-Caucasian cohorts. *Mult. Scler. Relat. Disord.* **17**, 87–91 (2017).
- Misu, T. et al. Presence of six different lesion types suggests diverse mechanisms of tissue injury in neuromyelitis optica. *Acta Neuropathol.* **125**(6), 815–827 (2013).

7. Nakamura, M. et al. Early high-dose intravenous methylprednisolone is effective in preserving retinal nerve fiber layer thickness in patients with neuromyelitis optica. *Graefes Arch. Clin. Exp. Ophthalmol.* **248**(12), 1777–1785 (2010).
8. Uzawa, A., Oertel, F. C., Mori, M., Paul, F. & Kuwabara, S. NMOSD and MOGAD: An evolving disease spectrum. *Nat. Rev. Neurol.* **20**, 602–619 (2024).
9. Rizzo, J. F., Andreoli, C. M. & Rabinov, J. D. Use of magnetic resonance imaging to differentiate optic neuritis and nonarteritic anterior ischemic optic neuropathy. *Ophthalmology* **109**(9), 1679–1684 (2002).
10. Miller, A., Green, M. & Robinson, D. Simple rule for calculating normal erythrocyte sedimentation rate. *Br. Med. J. (Clin. Res. Ed.)*. **286**(6361), 266 (1983).
11. Huang, L., Wang, Y. & Zhang, R. Retina thickness in clinically affected and unaffected eyes in patients with aquaporin-4 immunoglobulin G antibody seropositive neuromyelitis optica spectrum disorders: A systematic review and meta-analysis. *J. Neurol.* **270**(2), 759–768 (2023).
12. Chen, J. J. et al. OCT retinal nerve fiber layer thickness differentiates acute optic neuritis from MOG antibody-associated disease and multiple sclerosis: RNFL thickening in acute optic neuritis from MOGAD versus MS. *Mult. Scler. Relat. Disord.* **58**, 103525 (2022).
13. Cohen, J. A. 2024 revision of the McDonald diagnostic criteria for MS: Substantial and substantive changes. *Mult Scler.*13524585251351860 (2025).
14. Amanollahi, M. et al. Optical coherence tomography angiography measurements in neuromyelitis optica spectrum disorder and myelin oligodendrocyte glycoprotein antibody disease: A systematic review and meta-analysis. *Mult. Scler. Relat. Disord.* **91**, 105864 (2024).
15. Sugiyama, T., Araie, M., Riva, C. E., Schmetterer, L. & Orgul, S. Use of laser speckle flowgraphy in ocular blood flow research. *Acta Ophthalmol.* **88**(7), 723–729 (2010).
16. Tamaki, Y., Araie, M., Kawamoto, E., Eguchi, S. & Fujii, H. Noncontact, two-dimensional measurement of retinal microcirculation using laser speckle phenomenon. *Invest. Ophthalmol. Vis. Sci.* **35**(11), 3825–3834 (1994).
17. Luft, N. et al. Measurements of retinal perfusion using laser speckle flowgraphy and Doppler optical coherence tomography. *Invest. Ophthalmol. Vis. Sci.* **57**(13), 5417–5425 (2016).
18. Yamaguchi, C. et al. Differentiating optic neuropathies using laser speckle flowgraphy: Evaluating blood flow patterns in the optic nerve head and peripapillary choroid. *Acta Ophthalmol.* **103**, e49–e57 (2024).
19. Jarius, S. et al. Neuromyelitis optica. *Nat. Rev. Dis. Primers.* **6**(1), 85 (2020).
20. Lennon, V. A., Kryzer, T. J., Pittock, S. J., Verkman, A. S. & Hinson, S. R. IgG marker of optic-spinal multiple sclerosis binds to the aquaporin-4 water channel. *J. Exp. Med.* **202**(4), 473–477 (2005).
21. Lennon, V. A. et al. A serum autoantibody marker of neuromyelitis optica: Distinction from multiple sclerosis. *Lancet* **364**(9451), 2106–2112 (2004).
22. Takeshita, Y. et al. New BBB model reveals that IL-6 blockade suppressed the BBB disorder, preventing onset of NMOSD. *Neurol. (R) Neuroimmunol. Neuroinflamm.* **8**(6), e1076 (2021).
23. Takai, Y. et al. Staging of astrocytopathy and complement activation in neuromyelitis optica spectrum disorders. *Brain* **144**(8), 2401–2415 (2021).
24. Aboul-Enein, F. et al. Preferential loss of myelin-associated glycoprotein reflects hypoxia-like white matter damage in stroke and inflammatory brain diseases. *J. Neuropathol. Exp. Neurol.* **62**(1), 25–33 (2003).
25. Fujihara, K. et al. Interleukin-6 in neuromyelitis optica spectrum disorder pathophysiology. *Neurol. (R) Neuroimmunol. Neuroinflamm.* **7**, e841 (2020).
26. Wei, Y. et al. Cytokines and tissue damage biomarkers in first-onset neuromyelitis optica spectrum disorders: Significance of interleukin-6. *NeuroImmunoModulation* **25**(4), 215–224 (2018).
27. Oertel, F. C. et al. Retinal ganglion cell loss in neuromyelitis optica: A longitudinal study. *J. Neurol. Neurosurg. Psychiatr.* **89**(12), 1259–1265 (2018).
28. Zeka, B., Lassmann, H. & Bradl, M. Müller cells and retinal axons can be primary targets in experimental neuromyelitis optica spectrum disorder. *Clin. Exp. Neuroimmunol.* **8**(1), 3–7 (2017).
29. Steiner, E. et al. Loss of astrocyte polarization upon transient focal brain ischemia as a possible mechanism to counteract early edema formation. *Glia* **60**(11), 1646–1659 (2012).
30. Cacciaguerra, L. & Flanagan, E. P. Updates in NMOSD and MOGAD diagnosis and treatment: A tale of two central nervous system autoimmune inflammatory disorders. *Neurol. Clin.* **42**(1), 77–114 (2024).
31. Jayakumar, N., Lerch, M., Dale, R. C. & Ramanathan, S. MOG antibody-associated optic neuritis. *Eye (Lond)*. **38**(12), 2289–2301 (2024).
32. Hashimoto, R., Oyamada, M. & Maeno, T. Analysis of optic nerve head circulation using laser speckle flowgraphy in a case of pediatric optic neuritis. *EC Ophthalmol.* **9**, 572–581 (2018).
33. Kiyota, N. et al. Utility of laser speckle flowgraphy-derived vascular cloud for differentiating poor image quality data. *Nippon Ganka Gakkai Zasshi* **127**(5), 549–556 (2023).
34. Srikajon, J., Siritho, S., Ngamsombat, C., Prayoonwivat, N., Chirapapaisan, N., Siriraj Neuroimmunology Research Group. Differences in clinical features between optic neuritis in neuromyelitis optica spectrum disorders and in multiple sclerosis. *Mult. Scler. J. Exp. Transl. Clin.* **4**(3):2055217318791196 (2018).
35. Veto, S. et al. Inhibiting poly(ADP-ribose) polymerase: A potential therapy against oligodendrocyte death. *Brain* **133**(Pt 3), 822–834 (2010).
36. Mealy, M. A. et al. Longitudinally extensive optic neuritis as an MRI biomarker distinguishes neuromyelitis optica from multiple sclerosis. *J. Neurol. Sci.* **355**(1–2), 59–63 (2015).
37. Nielsen, H. H. et al. The urine proteome profile is different in neuromyelitis optica compared to multiple sclerosis: A clinical proteome study. *PLoS ONE* **10**(10), e0139659 (2015).
38. Liu, C. et al. Optical coherence tomography angiography helps distinguish multiple sclerosis from AQP4-IgG-seropositive neuromyelitis optica spectrum disorder. *Brain Behav.* **11**(5), e02125 (2021).
39. Liu, C. et al. Combination of serum markers with optical coherence tomography angiography for evaluating neuromyelitis optica spectrum disorders and multiple sclerosis. *Mult Scler. Relat. Disord.* **85**, 105478 (2024).
40. Rogaczewska, M., Michalak, S. & Stopa, M. Differentiation between multiple sclerosis and neuromyelitis optica spectrum disorder using optical coherence tomography angiography. *Sci. Rep.* **11**(1), 10697 (2021).
41. Wang, L., Cull, G. A., Piper, C., Burgoyne, C. F. & Fortune, B. Anterior and posterior optic nerve head blood flow in nonhuman primate experimental glaucoma model measured by laser speckle imaging technique and microsphere method. *Invest. Ophthalmol. Vis. Sci.* **53**(13), 8303–8309 (2012).
42. Aizawa, N. et al. Laser speckle and hydrogen gas clearance measurements of optic nerve circulation in albino and pigmented rabbits with or without optic disc atrophy. *Invest. Ophthalmol. Vis. Sci.* **55**(12), 7991–7996 (2014).
43. Takahashi, T. et al. Anti-aquaporin-4 antibody is involved in the pathogenesis of NMO: A study on antibody titre. *Brain* **130**(Pt 5), 1235–1243 (2007).
44. Sato, D. K. et al. Distinction between MOG antibody-positive and AQP4 antibody-positive NMO spectrum disorders. *Neurology* **82**(6), 474–481 (2014).
45. Banwell, B. et al. Diagnosis of myelin oligodendrocyte glycoprotein antibody-associated disease: International MOGAD Panel proposed criteria. *Lancet Neurol.* **22**(3), 268–282 (2023).

46. Wingerchuk, D. M. et al. International consensus diagnostic criteria for neuromyelitis optica spectrum disorders. *Neurology* **85**(2), 177–189 (2015).
47. Thompson, A. J. et al. Diagnosis of multiple sclerosis: 2017 revisions of the McDonald criteria. *Lancet Neurol.* **17**(2), 162–173 (2018).
48. Kiyota, N. et al. The impact of intraocular pressure elevation on optic nerve head and choroidal blood flow. *Invest. Ophthalmol. Vis. Sci.* **59**(8), 3488–3496 (2018).
49. Yamaguchi, C. et al. Evaluation of blood flow in arteritic anterior ischemic optic neuropathy using laser speckle flowgraphy: A case series. *Am. J. Ophthalmol. Case Rep.* **38**, 102316 (2025).
50. Hor, J. Y. et al. Epidemiology of neuromyelitis optica spectrum disorder and its prevalence and incidence worldwide. *Front. Neurol.* **11**, 501 (2020).

Acknowledgements

The authors thank Mr. Tim Hilts for reviewing and editing the manuscript's language. We thank Kenji Okamoto of Softcare Co., Ltd. for his valuable comments on the manuscript. This work was presented at the 128th Annual Meeting of the Japanese Ophthalmological Society on April 18, 2024. Financial support for this research was provided in part by the Japan Society for the Promotion of Science (JSPS) KAKENHI Grants-in-Aid for Scientific Research (B) (grant number: 17H04349; recipient: T.N.) and grants from the Center of Innovation Program (COI-NEXT) by the Japan Science and Technology Agency (JST) (grant number: JPMJPF2201). The funders had no role in the design or conduct of the study, collection, management, analysis, or interpretation of the data, preparation, review, or approval of the manuscript, or the decision to submit the manuscript for publication.

Author contributions

Contributions: CY, NK, NH, TM, KK, MA and TN conceived and designed the study. CY, NK and AT conducted the statistical analysis. CY, NK, NH, TM, KK, AT, MA and TN wrote the original manuscript. CY, NK, MO, TO, RK, KO, ST and TN contributed to the data collection and provided technical support. All authors verified the integrity and reproducibility of the results. All authors critically edited and approved the final version of the manuscript. TN is the guarantor of this work, has full access to all the data in the study and takes responsibility for the integrity of the data and the accuracy of the data analysis.

Declarations

Competing interests

The authors declare no competing interests.

Additional information

Supplementary Information The online version contains supplementary material available at <https://doi.org/10.1038/s41598-025-19110-7>.

Correspondence and requests for materials should be addressed to T.N.

Reprints and permissions information is available at www.nature.com/reprints.

Publisher's note Springer Nature remains neutral with regard to jurisdictional claims in published maps and institutional affiliations.

Open Access This article is licensed under a Creative Commons Attribution-NonCommercial-NoDerivatives 4.0 International License, which permits any non-commercial use, sharing, distribution and reproduction in any medium or format, as long as you give appropriate credit to the original author(s) and the source, provide a link to the Creative Commons licence, and indicate if you modified the licensed material. You do not have permission under this licence to share adapted material derived from this article or parts of it. The images or other third party material in this article are included in the article's Creative Commons licence, unless indicated otherwise in a credit line to the material. If material is not included in the article's Creative Commons licence and your intended use is not permitted by statutory regulation or exceeds the permitted use, you will need to obtain permission directly from the copyright holder. To view a copy of this licence, visit <http://creativecommons.org/licenses/by-nc-nd/4.0/>.

© The Author(s) 2025